Characterization of sub-cycle Electromagnetic pulse by long-life traces of wavefronts sampled in attosecond-level step

Hai Lin (linhai@siom.ac.cn)
Shanghai Institute of Optics and Fine Mechanics

Chengpu Liu
Shanghai Institute of Optics and Fine Mechanics

Research Article

Keywords:

Posted Date: April 19th, 2022

DOI: https://doi.org/10.21203/rs.3.rs-1410586/v2

Characterization of sub-cycle Electromagnetic pulse by long-life traces of wavefronts sampled in attosecond-level step

Hai Lin* and and Chengpu Liu†
State Key Laboratory of High Field Laser Physics,
Shanghai Institute of Optics and Fine Mechanics,
-P. O. Box 800-211, Shanghai 201800,China.
correspondence to: linhai@siom.ac.cn, chpliu@siom.ac.cn.
(Dated: March 26, 2022)

Current methods of characterizing electromagnetic(EM)-pulse can be divided into two classes, one is based on photons replica of the EM-pulse under test and the other on electrons replica. Methods in first class, such as interferometry and spectrography, are difficult to be competent for characterization of EM-pulse with attosecond(AS)-level duration due to too short duration or too broad bandwidth. Methods in second class, such as streak camera method, is competent but demands the pulse to have a peak strength high enough for efficiently producing X-ray photons. We propose a simple, universal method without special demand on the peak strength. It uses conventional optics method to sample, in AS-level step, wavefronts of the EM-pulse under test. Phase information carried by each sampled wavefront is fixed into, as a long-life trace, solid-state circuit and hence allow recording raw measurement data to be conducted over a feasible longer time scale.

Characterization of Electromagnetic(EM)-pulse involves in measuring pulse's intensity information and phase one [1,2]. Interferometry deals with fringes between photons replicas of the EM-pulse under test to retrieve/reconstruct its phase information. Because the fringe is a "volatile" trace, where the phrase "volatile" refers to the fringe disappearing once the EM-pulse is turned off, the interferometry is of less applicability to the characterization of ultrashort EM-pulse with a time duration T_d down to femto-second (fs) level because recording raw measurement results within $1fs$ time scale is impossible, (even for merely measuring fringes), for most photoelectric detectors whose fastest response time are usually at nanosecond(ns)-level. Spectrography also faces a difficulty in recording phase information due to lack of photodetectors and spectrographic materials of sufficiently broad bandwidth necessary for responding to ultrashort EM-pulse [1]. Therefore, "fixable" long-life traces are crucial for the characterization of $T_d < 1fs$ pulse or shorter and have been utilized in characterizing high-strength ultrashort EM-pulse (because producing such traces demands the EM-pulse to ionize matter). Here, we demonstrate that a universal method, without needing ionization, of characterizing $T_d < 1fs$ pulse through long-life traces fixed into solid-state circuit.

Some typical methods such as FROG [3-5], SPIDER [6], MIIPS[7], and D-Scan[8] are based on interferometry and spectrography. They are not direct measurements of EM-pulse under test with a photodetector, but encode the pulse information through nonlinear signal in different strategies. Although they can measure the pulse with precision well below the period for the carrier frequency and below the femtosecond scale, they do not measure the carrier envelope phase (CEP) of the pulse.

Therefore, people begin to utilize electrons replica of the EM-pulse under test to achieve the characterization [9-19]. The electrons replica can lead to a "fixable" trace, which allows recording raw measurement results, the input information for computer retrieval of phase information, over a realistic long time scale. In earlier works [9,10], characterization of the EM-pulse with ps-level T_d hires a two-color combination of EM beams. An optics-frequency(OF) beam is responsible for photo-ionizing atoms/molecules in gas phase, (or "create an electron replica of" the OF beam [11]), and a radio-frequency(RF) fields is responsible for mapping longitudinal positions of electrons into different impacting positions on a fluorescence screen parallel to the transverse direction [9,10]. These impacting positions are fixed traces (because secondary fluorescence radiation from them can finally, through a matured procedure, lead to resolved fixed traces on mass spectrometer). Such an OF+RF combination can achieve ps-level resolution [9,10]. Following similar idea or same principle, a X-ray+OF combination is hired in so-called atomic streak camera method [11-24]. It can characterize the EM-pulse with attosecond(AS)-level T_d [11-24], where the OF beam in the OF+RF combination is replaced by the X-ray beam and the RF fields is replaced by the OF fields. In an improved version of the streak camera method, producing electrons replica has been extended to be from solid materials instead of gas materials [25]

These methods require the strength of EM-pulse under test comparable to that of atomic electric field in order to enable 1) nonlinear optics crystal to exert marked modulation on a photon replica of the EM-pulse under test [3-8]; 2)atoms/molecules in gas phase to produce electrons replica (with sufficient total charge)[9-23]. It is appealing to develop a more universal method without special requirement on the strength and hence applicable to characterize those low-strength AS EM-pulse. Such a motive arises from realistic applications such as detecting/probing ultrafast

process taking place in chemical reactions among atoms/molecules in gas phase [20]. If achieving this goal through actively applying AS EM-pulses to the region where the reaction takes place, we will inevitably encounter a realistic question: synchronization between the detecting EM-pulse and the detected time-varying electron cloud (e-cloud). Because the detecting AS EM-pulse produced through above-mentioned routes have a central wavelength λ_{ctr} at X-ray range, it is not easy to keep the detected under long-time irradiation by the detecting. If choosing the detected under short-time irradiation by the detecting, the detecting must be able to well capture marked time-varying stages of the history of the detected. But it is difficult to predict when these marked time-varying stages start. Consequently, it is easy for the detecting with a short duration to miss these stages. Moreover, for avoiding to affect the reaction, the probing EM-pulse is also expected to have a sufficiently low strength and a spectrum well separated from level-spaces of reacting quantum systems (for avoiding resonant absorption). Although it is in principle capable of preventing the detecting from missing these stages by measures of synchronization, there are considerable difficulty in solving these problems. This is because both producing the detecting X-ray beam and the detected reaction involve in atoms/molecules in gas phase, in which particles' thermal motions increase the difficulty in synchronizing the detecting and the detected.

These factors enable RF pulse to be more suitable to act as such a detecting than its X-ray counterpart. When a RF EM-pulse with a vector potential $A^0 \sim exp\left(-i\omega_0 t\right)$ and $\omega_0 < MHz$, is incident on the time-varying density profile of an e-cloud $\left|\psi\left(t\right)\right|^2 \sim exp\left(t/\tau_{de}\right)$, there will be scattered/diffracted EM-signals $A^1 \sim \left|\psi\left(t\right)\right|^2 A^0 \sim exp\left(-i\left[\omega_0 + 1/\tau_{de}\right]t\right)$, which acts as the record/movie of the reaction. If the characteristic time scale of the e-cloud deformation τ_{de} is at fs-level (because of eV-level energy gap between levels, the transition time is therefore at fs-level), these diffracted signals are therefore be "up scattered" to have a shorter wavelength $1/\lambda^s_{ctr} = 1/\lambda^i_{ctr} + 1/\left[c\tau_{de}\right]$, which is within the OF regime. This fact can be illustrated by wave equation $4\pi\mu_0 e|\psi\left(t,r\right)|^2 A = \left[\nabla^2 - \partial_{tt}\right]A$. If not applying the detecting A_0, the strength of diffracted (OF) signals might be too weak to be detected. More important, the detected under long-time irradiation by the RF detecting is both technically and economically feasible. After all, keeping the reaction region long-time irradiated by an X-ray beam is too expensive and technically difficult.

Above discussion clearly explain why a more universal method, through cheaply-produced fixed traces, of characterizing AS EM-pulse is desirable. Next, we will expound this method.

Fig.1 displays several similar methods of "allocating" an pulse into different slices. An oscillating plane mirror can reflect temporal slices of an obliquely $(\pi/4)$ incident OF pulse into paths/rays of different transverse coordinates. These "detached" slices can be further amplified by beam expander such as a pair of co-focus concave lens and convex lens. Because each slice has a transverse size (up to 10λ-level for general Gaussian pulse), many parts from different slices "overlap" along a path and hence arrive a display unit mentioned latter (see Fig.1). If the oscillating mirror is curved instead of planar, slices are mapped into rays having not only different transverse coordinates but also their respective angles relative to the x-axis, a reference normal to the ray corresponded by the $\xi = \xi^0$ slice. Thus, the "overlap" of slices can be removed and slices are mapped into a bundle (of rays) with an angle spread $[\theta_{min}, \theta_{max}]$. In practice, available oscillating velocity can be at $10m/s$-level. For an oscillating curved mirror with an elliptic cross-section $\frac{x^2}{l^2} + \frac{[y+\beta(t)]^2}{h^2} = 1$, its intersection with a ray grazing incident along x-direction oscillates on the ellipse, and so do tangent and normal at the intersection. As illustrated by Fig.(1.b), the direction of reflected ray is $\pi - 2\theta$, where $\theta = \arctan\frac{\sqrt{h^2-\beta^2}}{\beta}$ is the angle between the x-axis and the tangent. For $\frac{h}{2} - |\beta|_{max} \leq \beta \leq \frac{h}{2} + |\beta|_{max}$ and $|\beta|_{max} = 10^{-17}m, h = 10^{-7}m$, corresponding θ is $\in \left[\arctan\left(2\right) - 10^{-10}\pi, \arctan\left(2\right) + 10^{-10}\pi\right]$, a too narrow range with a width $\sim 10^{-10}\pi$. Therefore, further amplifying the generated angle spread is necessary and can be through conventional geometric optics method illustrated by Fig.(1.c). Because a pair of co-axially arranged convex lenz can lead to $\frac{\theta_2}{\theta_1} = \frac{\arctan w/f_2}{\arctan w/f_1} \sim \frac{f_1}{f_2}$, a series of such pairs can lead to $\frac{\theta_{N+1}}{\theta_1} = \prod_{i=1}^{N}\frac{\theta_{i+1}}{\theta_i} = \left[\frac{f_1}{f_2}\right]^N$. Thus, even if limited oscillating velocity of the curved mirror, a bundle of rays with sufficiently large angle spread is still available.

It is well-known that the operation principle of optics fiber is to utilize total internal reflection (TIR). A fiber can only allow those rays whose incident angles θ exceeding the critical angle of the fiber to pass and prohibit others. This fact also implies that the fiber has a function of "filtering" incident non-parallel light rays bundle. Therefore, the angle spread becomes narrower after the fiber.

This fact enlightens us to arrange two fibers in a complementary manner (see Fig.2.a). For a non-parallel bundle with an initial angle spread $[\theta_{min}, \theta_{max}]$, we can arrange the critical angle of the first fiber, θ^1_{cri}, to be $\in [\theta_{min}, \theta_{max}]$ and thus only rays with $\theta \in \left[\theta^1_{cri}, \theta_{max}\right]$ can pass. If the second fiber is arranged in a complementary manner, in which a larger incident angle to the first fiber corresponds to a smaller one to the second, such an arrangement enables θ^2_{cri} to be $\in \left[\tilde{\theta_{max}}, \tilde{\theta^1_{cri}}\right]$, where $\tilde{\cdot} = \frac{\pi}{2} - \cdot$, and thus only rays with $\theta \in \left[\theta^2_{cri}, \tilde{\theta^1_{cri}}\right]$ can pass. Suitable arrangement can ensure $|\theta^2_{cri} - \tilde{\theta^1_{cri}}|$ small enough and thus only a very small portion of the initial bundle can pass. Actually, large-angle bending a fiber can play similar effect. Moreover, as illustrated by Fig.(2.c) even for a multi-color incident ray, a fiber

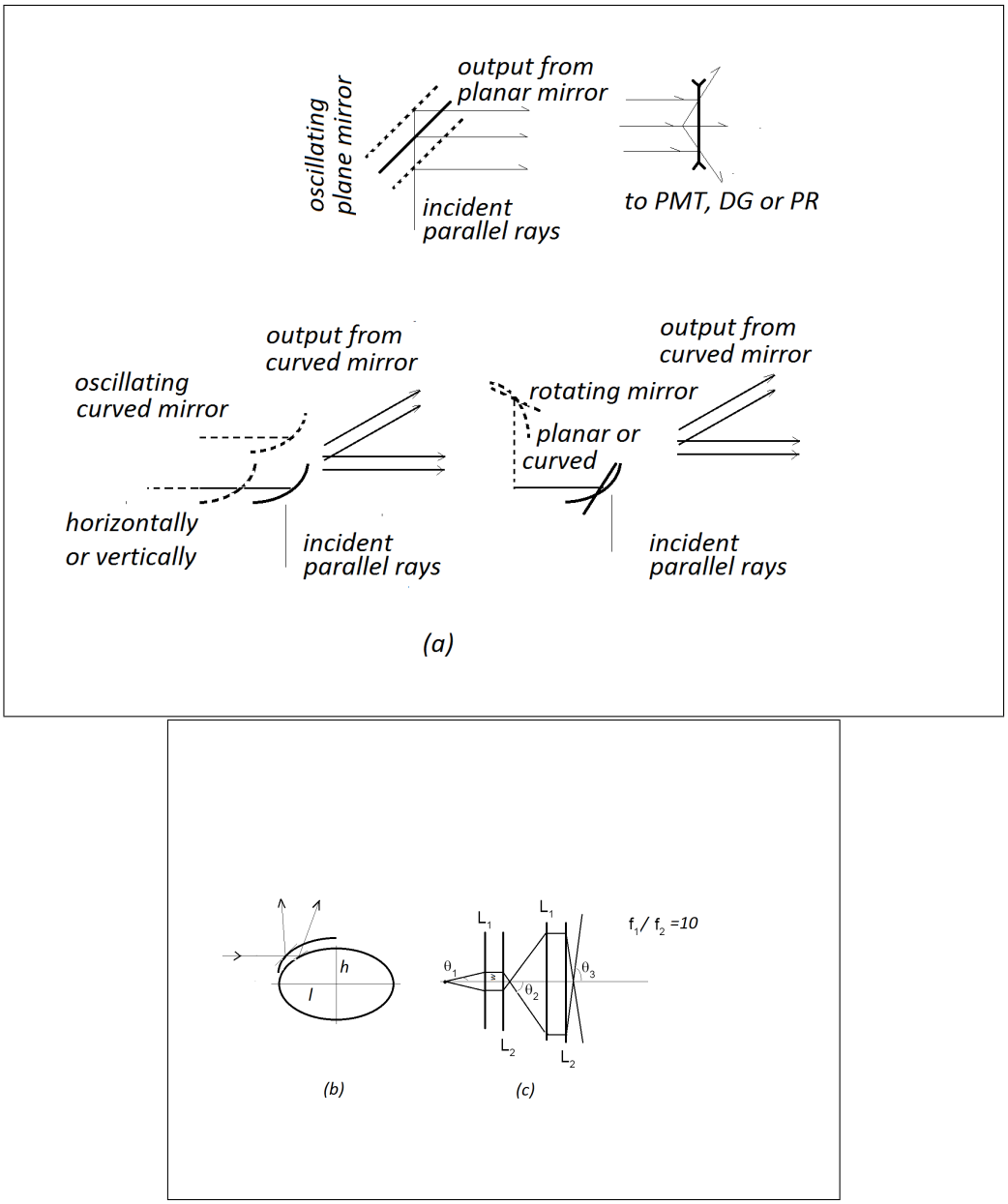

FIG. 1: (a)Upper panel ia the sketch of illustrating how temporal slices of an OF pulse are converted into parallel optics paths/rays with different transverse coordinates, where PMT stands for "photomultiplier tube", DG for the combination "diffraction grating+CCD" and PR for the combination "prism+CCD". They are "display units". Down panels are the sketches of illustrating similar ways of converting temporal slices into rays with different transverse coordinates and propagation direction angles (relative to a reference direction). These rays form a bundle with an angle spread. (b)Sketch illustrates angle spread generation from the reflection by an oscillating curved mirror. (c)Sketch illustrate angle spread amplification by a series of convex lenz co-axially arranged.

whose outer wall are coated with metal layer can cause the ray to have a larger transverse size and different color components to be of different transverse positions in a bundle of parallel rays. Consequently, above mechanism can still work for multi-color incident ray.

For sampling the $\xi = \xi^0$ slice, we can use a configuration arranged follows (see Fig.3): Because of small angle spread $|\theta^{max} - \theta^{min}|$, these rays can be nearly normal incident on a vacuum/medium, or $1/n_1$, interface. Other interfaces are also denoted in this manner, where $n_3 < n_2 < n_1$ are refractive indexes of mediums. Here, if $|\theta^{max} - \theta^{min}|$ on the $1/n_1$-interface is too small, we can magnify it through concave lens. Suitable angle between the n_1/n_2 interface and the x-axis, or $\angle 12$, enables those $\theta \geq \theta^{0+}$ rays to undergo a TIR on the n_1/n_2 interface. Those $\theta < \theta^{0+}$ rays

will have their respective transmitted replicas to be incident on the n_2/n_3 interface arranged with a specified value of $\angle 23 - \angle 12$. These transmitted slices/replicas have different values of the incident angle relative to the n_2/n_3 interface and thus those $\theta \leq \theta^{0-}$ rays will undergo a TIR. After the TIR twice, only the $\xi = \xi^0$ slice, or the $\theta = \theta^0$ path/ray, can have transmitted replica survived. The $n_3/1$ interface is arranged to be normal to the transmitted of the $\theta = \theta^0$ path/ray. The intensity of the $\theta = \theta^0$ ray can be calculated from that of the final transmitted and transmission ratios at these interfaces.

Using the n_4-medium is for ensuring those $\theta \leq \theta^{0-}$ rays to be "constrained" within the n_2-medium. At the $n1/n5$ interface and the $n2/n4$ interface, the TIR can occur for suitable values of n_4 and n_5. Thus, such a medium configuration can filter out the ray corresponded by the $\xi = \xi^0$ slice to be along the $n2/n3$ interface. More interest, if globally rotating this configuration, the $n0/n1$ interface will be normal to another ray $\in \left[\theta^{min}, \theta^{max}\right]$ and hence another slice will be finally filter out.

The n_2, n_3 media can be in solid-state, and others can be in liquid-state. For two classes of solid-state materials, crystal materials are anisotropic while glass materials are isotropic. Considering special requirements on geometric shapes of the n_2, n_3 media, we choose them made of glass materials (because they are easier to be processed than crystal materials). Available glass materials can be found elsewhere [21]: such as SF5,10,11 glasses (by SCHOTT AG).

Such a medium configuration enables directly detecting an interior slice (free from pollution by outer/earlier slices) to be feasible. A target-designed refractive index configuration "kit" (see Fig.2.b) can split an initial angle spread into 3 parts well separated spatially, one is of nearly zero angle spread and others still have large angle spread. According to Fig.2.b, central propagation direction of the zero angle spread part is downward, and those of others are leftward and rightward respectively. We can arrange "kits" to further filter leftward and rightward parts. Repeating this layout, we can build a series of "filtering", or a "kit tree". The output from each end of this "tree" corresponds to a slice of the initial beam. Each end can have its own display unit.

An OF transversely shaped wavefront can fix a trace on a power-frequency (PF) circuit. As illustrated by Fig.4.a, even for a 0-thickness slice, or a wavefront, it will still spend a considerable length of time to interact with a reflecting plane mirror. During this stage, because of the 0-thickness, there is always a straight-line of the metallic mirror, (which has a length $\sqrt{W^2 - z^2}$ and is perpendicular to the paper plane in Fig.4.a, and hence exhibits as a point), to contact with the slice and hence feel a parallel-to-plane electric field $E_{\parallel}$. If the metallic mirror is a part of a solid-state circuit, time-varying electric field $E_{\parallel}$ will drive a current within the circuit.

From $E_{\parallel}(t) = \frac{\sqrt{I}}{\sqrt{2}}\{cos\phi_s * C_c - sin\phi_s * C_s\}$, where

$$C_{c,s} = \int\int exp\left(-\rho^2/W^2\right)[cos, sin]\left(kz - \omega\frac{z}{\upsilon_g}\right)\delta\left(\rho - z\right)\delta\left(t - \frac{z}{\upsilon_g}\right)d\rho dz \tag{1}$$

and $k = \omega/c$, $2\pi\omega = c/\lambda_{ctr}$ and ϕ_s is the absolute phase, or the CEP, of the slice/wavefront, note that $C_c \neq 0$ (but $C_s = 0$) because of even (odd) integrated function, we can know accumulated charge $Q = \int\int jdtdS$, (where $j = \sigma E_{\parallel}$, dS is cross-section area of the skin layer of the wavefront and is equal to $skindepth \times \sqrt{W^2 - z^2}$ and σ is the conductivity of the metallic mirror)

$$Q = \frac{1}{2}\frac{\sqrt{I}}{\sqrt{2}}\sigma cos\phi_s \int exp\left(-\frac{\left(\omega - k\upsilon_g\right)^2 W^2}{4\upsilon_g^2}\right)\frac{W}{\upsilon_g}dS. \tag{2}$$

Note that the integral is $= 0$ when $W = 0$ and ∞. Some authors have noticed that similar charge accumulation (on electrode) effect associated with photocurrent in semiconductor depends on the CEP of the irradiating laser [26].

Thus, ϕ_s is, via a known triangular function, mapped into Q, which can be stored in the capacitor. When the wavefront is away, the circuit enters into a decay mode. The initial parameters, such as Q, determine time behavior of the decay mode. People can have sufficient time to record and analyze the decay mode and retrieve the Q-value. For example, if $\left[\sqrt{I}\right]_{V/m} \sim 10^0$ and $[W]_m \sim 10^{-6+1}$, $[\upsilon_g]_{m/s} = 2 \times 10^8$, $[S]_{m^2} \sim 10^{-12}$, $[\lambda_{ctr}]_m \sim 10^{-6}$, there will be $exp\left(-\frac{(\omega - k\upsilon_g)^2 W^2}{4\upsilon_g^2} = -25/16\right) \sim 0.21$ (if $W/\lambda_{ctr} = 5$ and $\upsilon_g/c = 2/3$), and because most metals can have a conductivity $\sigma \sim \left[\frac{1}{3}, 1\right] \times 10^6 \Omega^{-1} m^{-1}$ [27], there will be $[Q]_C \sim 10^{-19}$, the charge of an electron. For commercially available pF-level capacitor, there will be μV-level bias in the circuit. A transformer series can magnify such a weak bias to reach V-level and the decay mode starting from a V-level bias will take sufficiently long time to reach zero bias.

A wavefront will spend a considerable length of time $\frac{Th_c}{\upsilon_g}$ to transmit through a nonlinear optics crystal with a finite thickness Th_c, where υ_g is the group velocity in the crystal. Because the power P of harmonics pulse emitted

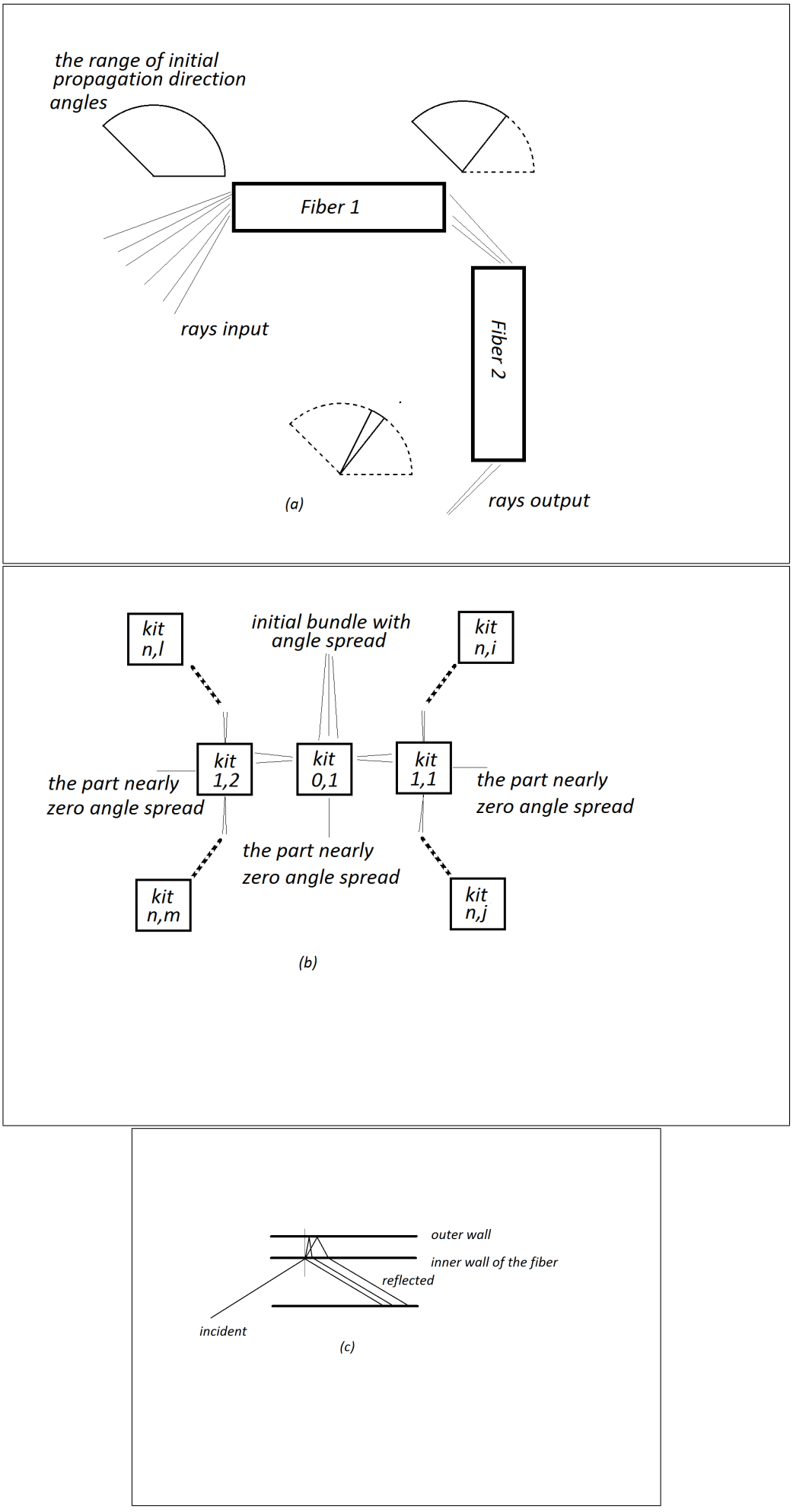

FIG. 2: (a)Sketch for illustrating how a kit composed of two fibers arranged in a complementary manner can filter out a slice. (b) Sketch for illustrating how similar kits (composed of composite mediums described latter) build up a hierarchic "tree" structure for sampling a pulse in a high resolution step. *kit* n, l refers to the l-th kit in the n-th level in the hierarchy, and $1 \leq l \leq 2^n$. (c) Sketch for illustrating the mechanism illustrated in (a) still work for mutli-color incident ray.

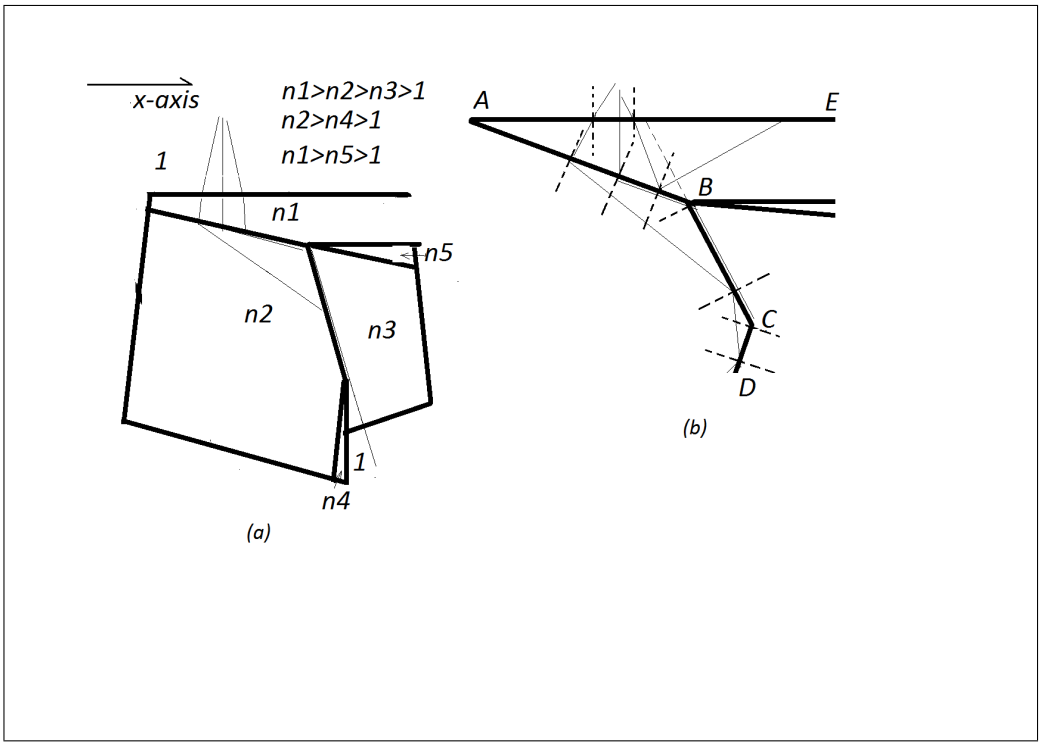

FIG. 3: Sketch for illustrating how the medium configuration can filter out a slice. (a) for displaying the medium configuration. (b) are the illustration based on ray-optics, where thick solid lines stand for interfaces, thin solid lines for light rays and dashed lines for normal lines of interfaces.

from the crystal is proportional to the electric field of the wavefront $\sqrt{I}$, the I-value of a wavefront can be derived by measuring the energy $P * \frac{Th_c}{v_g}$.

We have proposed a feasible scheme, which is based on conventional optics technique and completely based on solid-state components, of "sampling" slices/wavefronts of an OF EM-pulse in AS-level steps. It is through cheaply-produced fixable traces of the EM-pulse under test and does not require to ionize charge-neutral matter to produce electrons replica. The fixable traces have a simple, clear mathematics relation with the absolute phase of a wavefront and hence implies a direct measurement of phase information. Therefore, it is of universal applicability to characterization of low-strength ultrashort EM-pulse.

Acknowledgement

This work is supported by NSFC.Grant.No.12074398.

DATA AVAILABILITY

The data that supports the findings of this study are available within the article [and its supplementary material].

* Electronic address: linhai@siom.ac.cn
† Electronic address: chpliu@siom.ac.cn

[1] I. A. Walmsley and C. Dorrer, Adv. Opt. Photon. **1**, 308(2009) and refs therein.
[2] A. S. Wyatt, *et al*, Optica **3**, 303(2016)
[3] K. W. Delong, R. Trebino, J. Hunter and W. E. White, J. Opt. Soc. Am. B. **11**, 2206(1994).
[4] R. Trebino, K. W. Delong, D. N. Fittinghoff, J. N. Sweetser, M. A. Krumbugel, B. A. Richman and D. J. Kane, Rev. Instrum. **68**, 3277(1997).

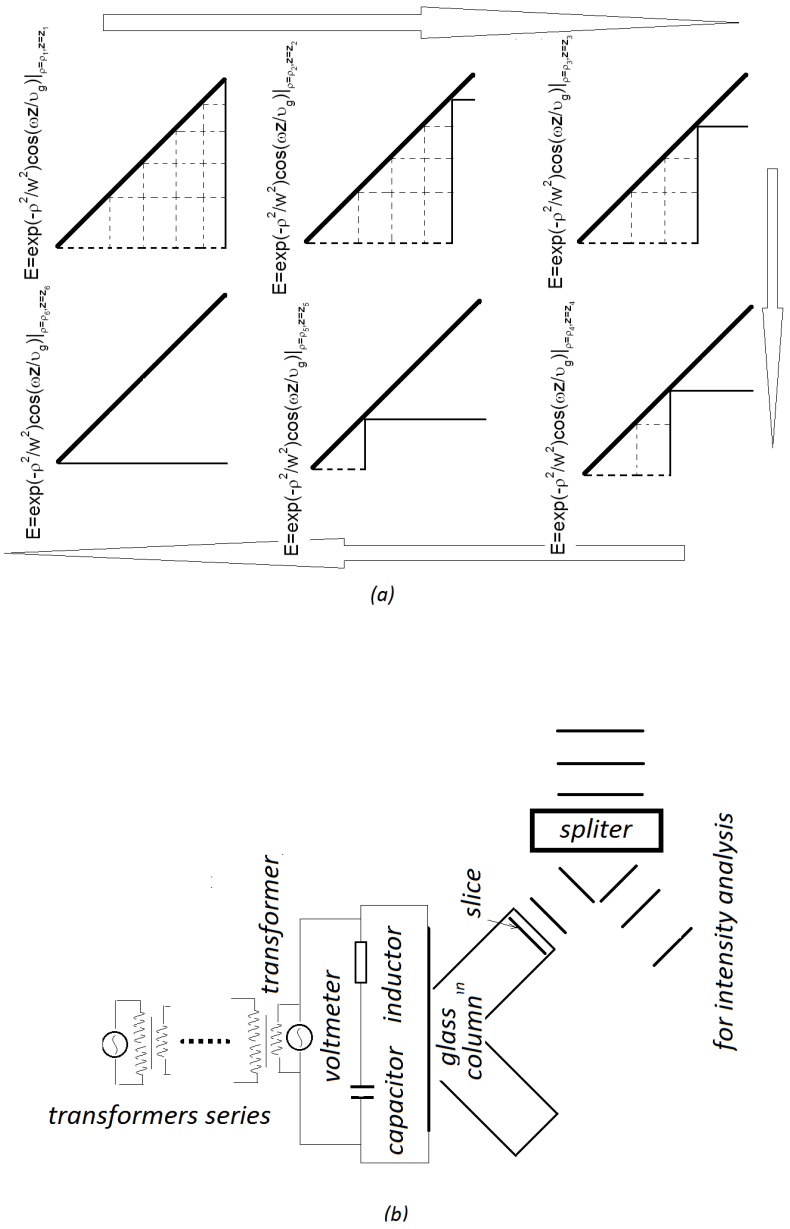

FIG. 4: Sketch for illustrating how to couple a slice of 0-thickness, or a wavefront, with a circuit. (a) for illustrating how an oblique-incident wavefront is reflected by a metallic plate coated on the truncated face of two cross-spliced un-doped glass columns. The thickest solid line stands for the metal mirror, the thinner solid lines for the wavefront segments, these thinnest dashed lines for future wavefront segments and paths. Three arrows direct time rising. (b) for illustrating that the metal mirror is a part of a source-less LC circuit. The voltmeter at the end of transformer series can be attached by pen and paper for fixing a permanent physical trace of the slice.

[5] Y. Mairesse and F. Quere, Phys. Rev. A. **71**, 011401(2005).
[6] C. Iaconis and I. A. Walmsley, Opt. Lett. **23**, 792(1998).
[7] V. V. Lozovoy, I. Pastirk, and M. Dantus, Opt. Lett. **29**, 775(2004).
[8] M. Miranda, Opt. Express. **20**, 18732(2012).
[9] D. J. Bradley, B. Liddy and W. E. Sleat, Opt. Commun. **2**, 391(1971).
[10] M. Ya. Schelev, M. C. Richardson and A. J. Alcock, Appl. Phys. Lett. **18**, 354(1971).
[11] E. Constant, V. D. Taranukhin, A. Stolow and P. B. Corkum, Phys. Rev. A. **56**, 3870(1997).
[12] M. Hentschel, *et al*, Nature. **414**, 509-513(2001).
[13] J. Itatani, F. Quere, G.L. Yudin, M.Y. Ivanov, F. Krausz, P.B. Corkum, Phys. Rev. Lett. **88**, 173903(2002).
[14] R. Kienberger, J. Stuart, B. Wyithe, A. Loeb, Nature. **427**, 817(2004).
[15] A. Scrinzi, M. Geissler and T. Brabec, Phys. Rev. Lett. **86**, 412(2001).
[16] E. Goulielmakis, Science **305**, 1267(2004).
[17] Ferenc Krausz and Misha Ivanov, Rev. Mod. Phys. **81**, 163 (2009) and refs therein.
[18] Peter Dombi, Zsuzsanna Papa, Jan Vogelsang, Sergey V. Yalunin, Murat Sivis, Georg Herink, Sascha Sch?fer, Petra Gro?, Claus Ropers, and Christoph Lienau, Rev. Mod. Phys. **92**, 025003(2020) and refs therein.
[19] J. Gagnon and V.S. Yakovlev, Appl. Phys. B. **103**, 303-309(2011). DOI 10.1007/s00340-010-4358-2
[20] A. Zewail, J. Phys. Chem. A **104**, 5660-5694(2000).
[21] https://refractiveindex.info and refereces therein.
[22] G. G. Paulus, F. Lindner, H. Walther, A. Baltuska, E. Goulielmakis, M. Lezius, and F. Krausz, Phys. Rev. Lett. **91**, 253004(2003).
[23] D. Milosevic, G. G. Paulus, D. Bauer, and W. Becker, J. Phys. B **39**, R203(2006).
[24] H. Wang, M. Chini, S. D. Khan, S. Chen, S. Gilbertson, X. Feng, H. Mashiko, and Z. Chang, J. Phys. B **42**, 134007 (2009).
[25] M. R. Bionta, F. Ritzkowsky, M. Turchetti, Y. Yang, D. C. Mor, W. P. Putnam, F. X. Kartner, K. K. Berggren and P. D. Keathley, Nat. Photonics **15**, 456 (2021).
[26] V. Hanus, *et. al*, Optica **8**, 570 (2021).
[27] K. Huang and R. Han, *Solid State Physics*, Higher-Education Press, China (1988).